RSC Advances

PAPER

View Article Online
View Journal | View Issue

Cite this: *RSC Adv.*, 2025, **15**, 50408

Synergistic anti-friction performance and lubricating film mechanism of erucamide and *N*-phenyl-α-naphthylamine in polyurea grease at elevated temperatures

Qingchun Liu,[a] Wuxin Yu,[*a] Yimin Mo,[b] Jun Wang,[c] Changye Liu,[c] Ye Hong,[a] Qiang Zhang[a] and Fengjie Chen[d]

Received 12th September 2025
Accepted 18th November 2025

DOI: 10.1039/d5ra06889d

rsc.li/rsc-advances

The synergistic effect of anti-wear and antioxidant additives in lubricating grease can effectively reduce friction and wear. In this study, a polyurea grease containing 2 wt% erucamide (ER) and 1 wt% *N*-phenyl-α-naphthylamine (*N*-PAN) was prepared, and its tribological performance on GCr15 steel at different temperatures was systematically investigated. The results show that the average friction coefficient of the grease with ER and *N*-PAN decreases by approximately 32% compared with the base polyurea grease, exhibiting the best tribological performance at 75 °C (average friction coefficient = 0.088). Surface characterization reveals that the synergistic action of ER and *N*-PAN promotes the formation of a dense and durable lubricating film. ER molecules form a bilayer structure, filling the voids of the base oil and transforming sliding friction into rolling friction, while *N*-PAN effectively inhibits oxidation and retards film degradation. This synergistic mechanism significantly enhances the high-temperature friction-reducing and antioxidative properties of the grease, demonstrating its potential for high-temperature mechanical lubrication applications.

1 Introduction

Greases are widely applied in mechanical components to reduce friction and wear, thereby ensuring efficient operation and prolonging service life.[1–3] However, the load-bearing capacity of grease films is limited, and temperature variations can lead to insufficient lubrication, further exacerbating wear in mechanical parts.[4–6] Traditional anti-wear additives, including sulfur-, phosphorus-, molybdenum-, and other metal-based compounds, improve tribological performance by forming protective oxide layers on metal surfaces, but their friction-reducing mechanisms are relatively simple, and the overall effect remains limited.[7–10] Recent advances in nanotechnology have promoted the development of novel anti-wear materials. Nanoparticles can exhibit multiple lubrication effects, forming protective chemical films on metal surfaces, while their small size allows them to embed into the lubricating film, contributing synergistically to friction reduction.[11–15] For example, Guo H. *et al.*[16] demonstrated that magnesium hydroxide–magnesium silicate nanoparticles act as self-repairing anti-wear agents, and 0.4 wt% hydroxide–magnesium silicate nanoparticles added to grease improved steel durability and reduced wear. Wu C. *et al.*[17] investigated lithium-based greases containing carbon black, Fe_3O_4, and Al_2O_3 nanoparticles and found that Al_2O_3 enhanced both tribological performance and vibration suppression in rolling bearings by forming a metallic film and promoting base oil flow. Similarly, Wu C. *et al.*[18] reported that adding 1 wt% CuO nanoparticles to calcium sulfonate or polyurea greases reduced friction coefficients and wear scar diameters, while polyurea grease with CuO significantly suppressed bearing vibrations. These studies indicate that the tribological performance of greases can be effectively enhanced by selecting nanoparticles with suitable physicochemical properties, highlighting the potential of nanomaterials for advanced lubrication applications.

With increasing environmental concerns, the development of eco-friendly additives that combine excellent friction-reducing performance with safety is highly desirable.[19,20] Erucamide, a two-dimensional nano-scale material, possesses a high melting point, good thermal stability (stable up to 273 °C), and non-toxicity, and is widely used as an anti-blocking, slip, anti-fouling, and dispersing agent in plastics and resins.[21–25] In polymer systems, erucamide migrates to the surface of films, effectively reducing the surface friction coefficient.[26–28] Y. Y. Di. *et al.*[29] reported that erucamide incorporated into self-

[a]School of Intelligent Manufacturing, Jianghan University, Wuhan, 430056, China. E-mail: feedback-ssm@jhun.edu.cn

[b]School of Mechanical and Electrical Engineering, Wuhan University of Technology, Wuhan, 430070, China

[c]SAIC-GM-Wuling Automobile Corporation, Liuzhou 454007, China

[d]State Key Laboratory of Precision Blasting, Jianghan University, Wuhan, 430056, China

assembled films (ER-SAF) exhibited pronounced atomic-scale stick–slip behavior and ultralow friction loss. These characteristics suggest that erucamide holds significant potential for enhancing the tribological performance of lubricating greases while maintaining environmental compatibility.

Despite these advances, base oils in greases are prone to oxidation, generating by-products such as aldehydes and carboxylic acids that increase friction and deteriorate lubrication.[30,31] Antioxidants are therefore essential to terminate free-radical chain reactions and prevent oxidative degradation. *N*-phenyl-α-naphthylamine (*N*-PAN), a high-temperature amine-based antioxidant, shows excellent stability in synthetic lubricants.[32,33] And Du S. D. *et al.*[34] confirmed that amino and alkyl groups enhance its antioxidant capacity.

In our previous work, to evaluate the tribological performance of polyurea greases containing different ratios of ER and *N*-PAN on GCr15 steel, a series of greases with ER/*N*-PAN ratios of (0, 0), (0, 3), (1, 2), (2, 1), and (3, 0) were prepared. The friction coefficients and wear morphologies of GCr15 steel lubricated by these five types of greases were systematically investigated. The results demonstrated that the tribological performance of the polyurea grease was significantly improved when 2 wt% ER and 1 wt% *N*-PAN were incorporated. Therefore, in this study, a formulation containing 2 wt% ER and 1 wt% *N*-PAN was selected to further investigate the tribological behavior under different temperature conditions.[35,36] however, the combined effects of ER and *N*-PAN on friction behavior at various temperatures and the underlying mechanisms remain unclear. Addressing this gap is critical for the rational design of high-performance, environmentally compatible greases.

In this work, for the first time, 2 wt% erucamide (ER) and 1 wt% *N*-phenyl-α-naphthylamine (*N*-PAN) were incorporated into polyurea grease to investigate their tribological performance under different temperatures. The structural features of the prepared grease were characterized to elucidate the organization of polyurea thickener fibers. Tribological tests were conducted on GCr15 steel lubricated with the greases, and the worn surfaces and cross-sections of the steel were analyzed to evaluate friction and wear behavior. Based on these experimental results, the underlying friction-reducing mechanisms of polyurea grease containing 2 wt% ER and 1 wt% *N*-PAN at various temperatures were systematically explored. This study provides fundamental insights into the design of high-performance, environmentally friendly greases with enhanced high-temperature tribological performance.

2 Materials and methods

2.1 Preparation and characterization of polyurea grease

2.1.1 Materials and preparation of polyurea grease. Polyurea grease was prepared by thickening a base oil with a polyurea thickener and incorporating functional additives. In this study, the base oil was a poly-α-olefin (PAO4) synthetic oil with a kinematic viscosity of 5.191 $mm^2\ s^{-1}$ at 100 °C, exhibiting excellent thermal stability and oxidative resistance. The base oil also possesses a high viscosity index, which facilitates the formation of a stable lubricating film. The PAO base oil was supplied by Sinopec. The polyurea thickener was synthesized *via* the reaction of methylene diphenyl diisocyanate (MDI) with cyclohexylamine, as illustrated in the following reaction scheme (1):In eqn (1), the green dashed box highlights the urea moiety.

The preparation of polyurea grease was carried out in five steps (as shown in Fig. 1a):

(1) The base oil was divided into two portions, with MDI and cyclohexylamine each dissolved in one portion under continuous stirring to obtain two separate solutions.

(2) The reaction vessel was preheated to 100 °C, and the two solutions were then introduced into the vessel and maintained at this temperature for 30 min. In the last 5 min, a small amount of distilled water was added to quench excess MDI.

(3) The reaction mixture was heated to 150 °C and maintained for an additional 30 min.

(4) The reaction vessel was allowed to cool to room temperature.

(5) The resulting mixture, together with the additives, was processed in a three-roll mill for grinding, homogenization, degassing, and filtration to obtain the final polyurea grease.

For sample identification, the grease was labeled as PG-ER-N(*e*, *n*), where PG denotes polyurea grease, ER represents erucamide, *N* denotes *N*-phenyl-α-naphthylamine, and *e* and *n* correspond to the mass fractions of ER and *N*-PAN, respectively.

2.1.2 Structural characterization of polyurea thickener. To observe the structural features of the polyurea thickener, it was first separated from the grease. The defatting and isolation procedure of the thickener was carried out as follows (as shown in Fig. 2a):

(1) 0.5 mL of grease was placed into a 2 mL centrifuge tube.

(2) 1 mL of petroleum ether was added to the tube to dissolve the grease completely.

(3) The centrifuge tube was placed in a centrifuge and spun at 7000 rpm for 30 min, followed by standing for 30 min. This step was repeated three times.

(4) The lower precipitate in the centrifuge tube was collected, and steps 2–4 were repeated three times to ensure complete removal of oil.

(5) The final precipitate was transferred onto a silicon wafer (10 mm × 10 mm) and dried.

(6) Under vacuum, the precipitate on the silicon wafer was coated with a thin layer of gold using an ion sputtering instrument. The sputtering time was 100 s and the process was repeated three times to obtain the solid polyurea thickener.

2.2 Tribological tests

The application background of this study is related to the optimization of grease lubrication in a vehicle chassis support bearing. The support bearing used is a deep groove ball bearing (model 6206), which contains approximately 6 g of grease per unit. To simulate the tribological behavior of the grease-lubricated contact in the bearing during operation, a reciprocating friction test was carried out using an MFT-5000 tribometer (Rtec Instruments, USA) (as illustrated in Fig. 1b and c), with a GCr15 steel block and a Si_3N_4 ball serving as the friction pair. The tribopair consisted of a GCr15 steel block and

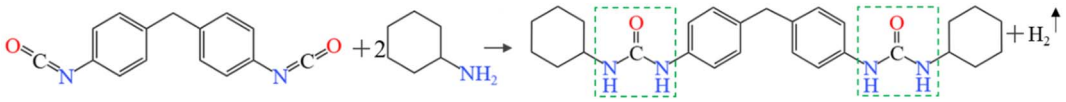

(1)

a Si_3N_4 ball. The GCr15 steel block had dimensions of 16 mm × 12 mm × 6 mm, and the Si_3N_4 ball had a diameter of 6.3 mm (the hardness of the GCr15 steel is approximately HRC 60 ± 2 (corresponding to Hv 700 ± 20), and that of the Si_3N_4 ball is Hv 1450 ± 50). Prior to testing, the GCr15 steel blocks were pretreated as follows: the blocks were polished for 30 min using 1200# and 2000# abrasive papers on a metallographic polishing machine (MP-1B). The surface roughness of each polished block was measured at 10 randomly selected locations using a 3D optical profilometer (UP-3D Rtec) to ensure an average roughness below 0.05 μm. Finally, all tribopairs were cleaned in an ultrasonic bath (YM-008T) with anhydrous ethanol for 10 min before testing.

The tribological tests were performed using a linear reciprocating motion, following the ASTM G133-05 (2016) standard, to simulate the friction process of a deep groove ball bearing. The GCr15 steel block and Si_3N_4 ball were mounted on separate fixtures, and a uniform layer of grease (~3 mm thickness (the grease layer thickness was set to 3 mm, which approximates the practical grease film thickness in bearing lubrication. This thickness also accounts for the open system configuration (non-sealed environment) of the test, ensuring sufficient grease contact and lubrication supply throughout the experiment)) was applied to the surface of the steel block. The testing conditions are summarized in Table 1. Additionally, a heating device and a temperature sensor were attached to the side of the GCr15 steel sample. To investigate the influence of temperature on the lubrication performance, tests were performed at 25 °C, 75 °C, and 120 °C, corresponding to ambient temperature, elevated operating temperature (*e.g.*, during summer vehicle operation), and extreme high-temperature conditions, respectively.

During the tests, the real-time variations of friction force and normal load were recorded by the sensors of the MFT-5000 tribometer at a data acquisition rate of 100 values per second. A total of 6000 friction coefficient values were collected per minute, and the average value over each 6 s interval was taken as the friction coefficient for the test. To ensure the reliability of the data, each test was repeated three times.

2.3 Surface analysis and characterization

After the tribological tests, the worn surfaces and cross-sections of the GCr15 steel blocks were examined using an electron probe microanalyzer (JAXA-8230, EPMA) and a field-emission scanning electron microscope (Zeiss Ultra Plus, FESEM) to investigate the wear mechanisms and the lubricating behavior of the grease. Elemental analysis of the worn surfaces was conducted using an X-ray energy dispersive spectrometer (Inca-X-ACT, EDS) to observe the elemental distribution and study the tribochemical reactions occurring on the wear surfaces. Surface topography and wear profile parameters of the GCr15 steel samples were measured using a 3D optical profilometer. For each sample, ten measurements were taken at different locations, and the average values were used as the final results.

3 Results and discussion

3.1 Structural characterization of polyurea thickener

The microstructure of the polyurea thickener was examined using a field-emission scanning electron microscope (FESEM) following the defatting procedure described in Section 2.1.2. Low- and high-magnification FESEM images of the defatted

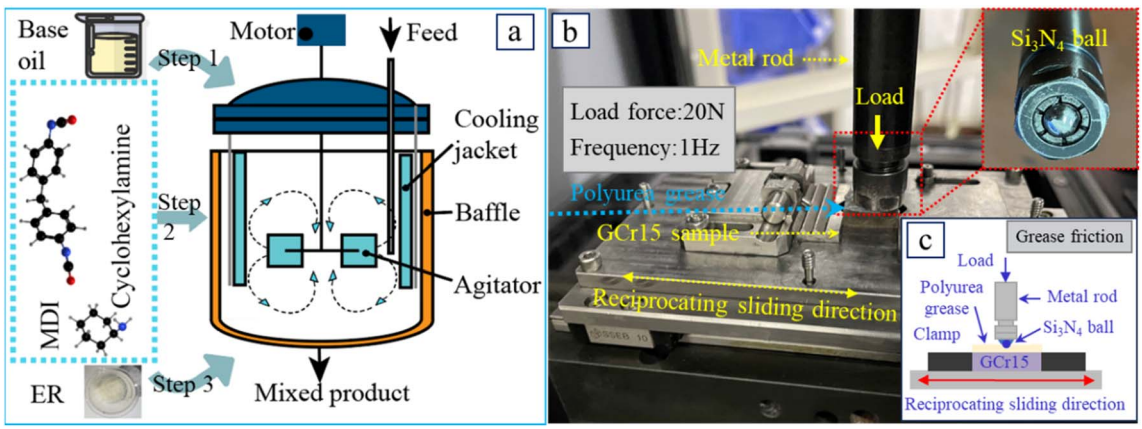

Fig. 1 Schematic illustration of polyurea grease preparation (a), MFT-5000 Rtec tribological testing system (b) and schematic diagram (c).

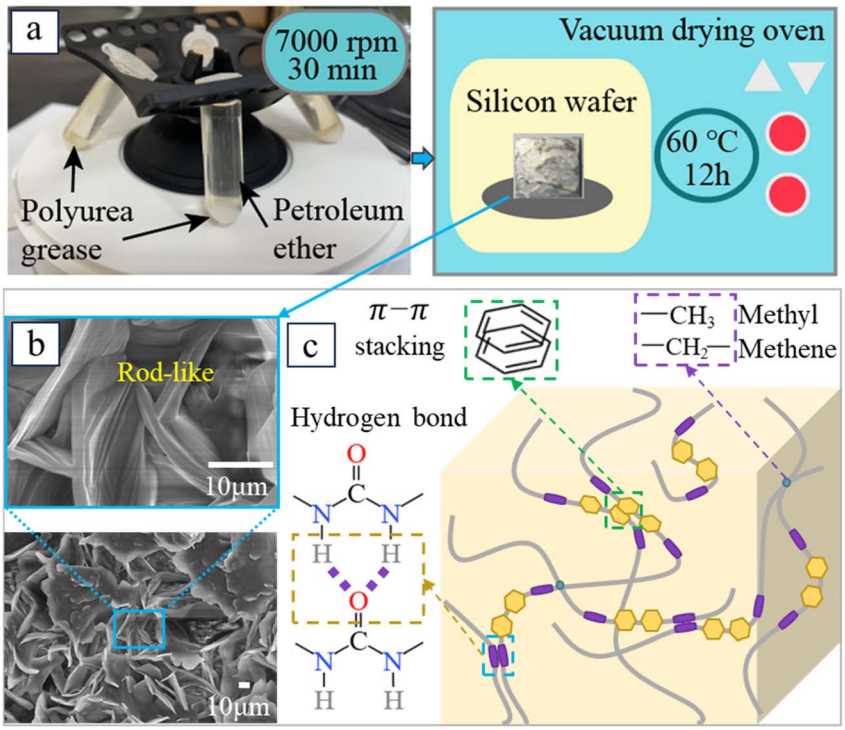

Fig. 2 Schematic illustration of polyurea grease degreasing process (a), low- and high-magnification FESEM images of the degreased polyurea thickener (b) and schematic of intermolecular interactions in polyurea grease (c).

thickener are shown in Fig. 2b. In polyurea grease, the molecules primarily aggregate through hydrogen bonding, π–π stacking, and van der Waals interactions. A schematic illustration of the intermolecular interactions in polyurea grease is presented in Fig. 2c.

As shown in Fig. 2b, the polyurea thickener consists of rod-like fibers of varying lengths, which tightly aggregate to form extensive lamellar structures. The thickener fibers synthesized from cyclohexylamine are primarily short rods, which gradually assemble into a dense supporting "skeleton" of the thickener.

From Fig. 2c, in the polyurea thickener, the molecules are primarily aggregated through non-covalent interactions such as hydrogen bonding, π–π stacking, and van der Waals forces. Among these, hydrogen bonding plays the dominant role in determining the tribological performance.[37] The hydrogen bond (N–H···O) is a strong intermolecular interaction, and its well-ordered hierarchical structure directly determines the thermodynamic–kinetic balance between structural preservation and adaptive reorganization during thermal processing, which is crucial for enhancing the self-healing efficiency of the polyurea thickener.[38–40] The π–π stacking interaction, existing between aromatic (C=C) bonds, contributes to the high-temperature stability and toughness of the polyurea structure.[41] The cooperative effect between π–π stacking and hydrogen bonding significantly enhances the mechanical strength of the material.[42] Meanwhile, van der Waals forces, which originate from the induced dipole interactions between adjacent methyl or methylene groups, are relatively weak but facilitate the uniform distribution of base oil within the thickener matrix.[43]

Due to these synergistic intermolecular interactions, rod-like fibers of different lengths can aggregate to form large-scale lamellar structures. When the applied shear stress exceeds the yield shear stress, hydrogen bonds, π–π stacking, and van der Waals interactions are disrupted, allowing the base oil to be released and form a lubricating film between the friction pairs. Once the shear stress is removed, the hydrogen bonds predominantly reform, assisted by π–π stacking and van der Waals forces, enabling the thickener network to self-reorganize, encapsulate the base oil, and rebuild a stable lubricating film that prevents direct contact between friction surfaces and effectively reduces friction.

3.2 Friction and wear effects of greases

Reciprocating sliding tests were conducted for 1800 s, with each test repeated three times. The average friction coefficient over each 6 s segment was taken as the representative value. The maximum and minimum friction coefficients within each test were used to define the error bars. The friction coefficients and

Table 1 The testing conditions

Reciprocating distance/mm	Reciprocating frequency/Hz	Test load (F_z)/N	Test time/min
8	1	20	30

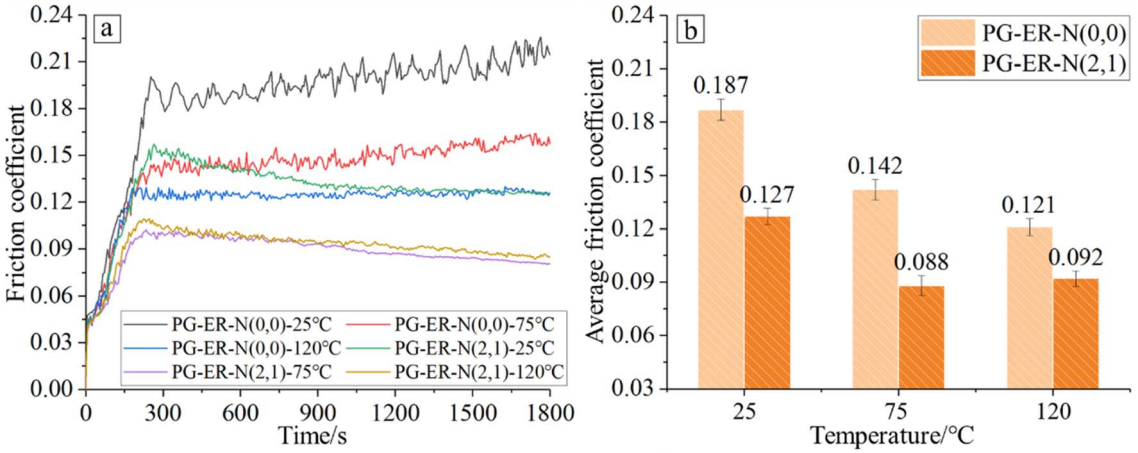

Fig. 3 Friction coefficients (a) and average friction coefficients (b) of GCr15 steel specimens lubricated with PG-ER-N series greases at different temperatures.

mean values of the PG-ER-N series greases lubricating the specimens at different temperatures are shown in Fig. 3.

As shown in Fig. 3, the friction coefficient of GCr15 steel lubricated with PG-ER-N(0, 0) grease decreases with increasing temperature, and the fluctuations in the friction coefficient curves also diminish, indicating improved anti-friction performance at higher temperatures. At the same temperature, the friction coefficient curve of PG-ER-N(2, 1) grease exhibits smaller fluctuations and lower friction values compared to PG-ER-N(0, 0), demonstrating that the anti-friction performance of PG-ER-N(2, 1) is superior. After the addition of ER and *N*-PAN, the average friction coefficient of the grease decreased significantly by approximately 32% compared to the base polyurea grease. Among the polyurea greases, PG-ER-N(2, 1) shows the best friction-reducing performance at 75 °C, with an average friction coefficient of 0.088. These results indicate that the incorporation of 2 wt% erucamide and 1 wt% *N*-phenyl-α-naphthylamine into polyurea grease effectively reduces friction and wear, with optimal tribological performance achieved at 75 °C.

From Fig. 4(a), under the 25 °C condition, severe spalling and pits are observed on the PG-ER-N(0, 0)-25 °C sample, indicating abrasive wear. Combined with the EDS results in Fig. 5(a1–a3), the presence of abundant O and Si elements suggests oxidative reactions and adhesive wear, noting that the Si content in GCr15 steel is approximately 21%.[44]

To investigate the tribological performance of the PG-ER-N series greases on GCr15 steel at different temperatures, the wear tracks on the sample surfaces after the tribological tests were analyzed. EPMA images of the GCr15 steel surfaces lubricated with the PG-ER-N series greases at various temperatures are shown in Fig. 4, and the corresponding EDS analyses are presented in Fig. 5.

As shown in Fig. 4, the wear on GCr15 steel surfaces lubricated with the PG-ER-N series greases varies with temperature, and the primary wear features are grooves and wear debris. At the same temperature, the wear on samples lubricated with PG-ER-N(2, 1) is less than that on samples lubricated with PG-ER-N(0, 0). For the same grease, surface wear decreases as the temperature increases. These results indicate that the anti-friction performance of PG-ER-

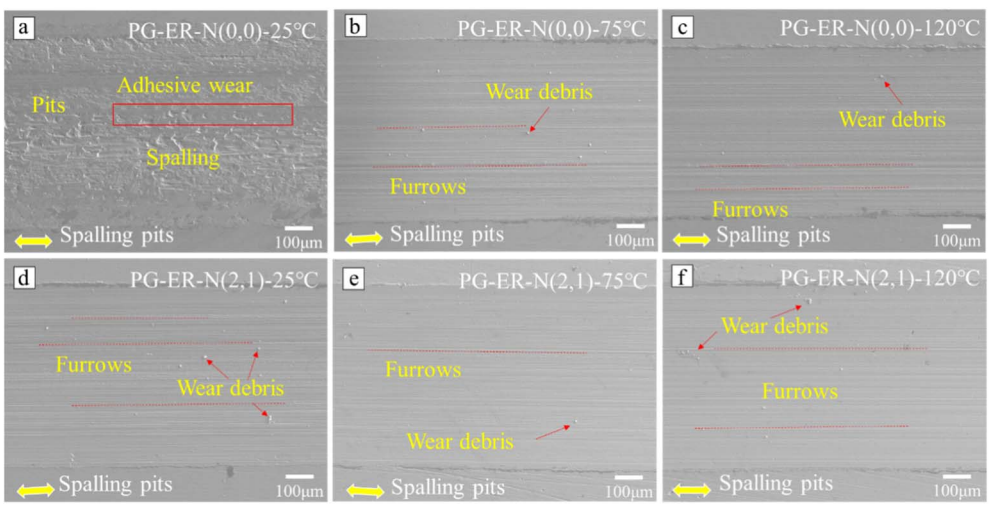

Fig. 4 EPMA images of the GCr15 steel surfaces lubricated with the PG-ER-N (0, 0) series greases (a–c) and PG-ER-N (2, 1) series greases (d–f) at different temperatures.

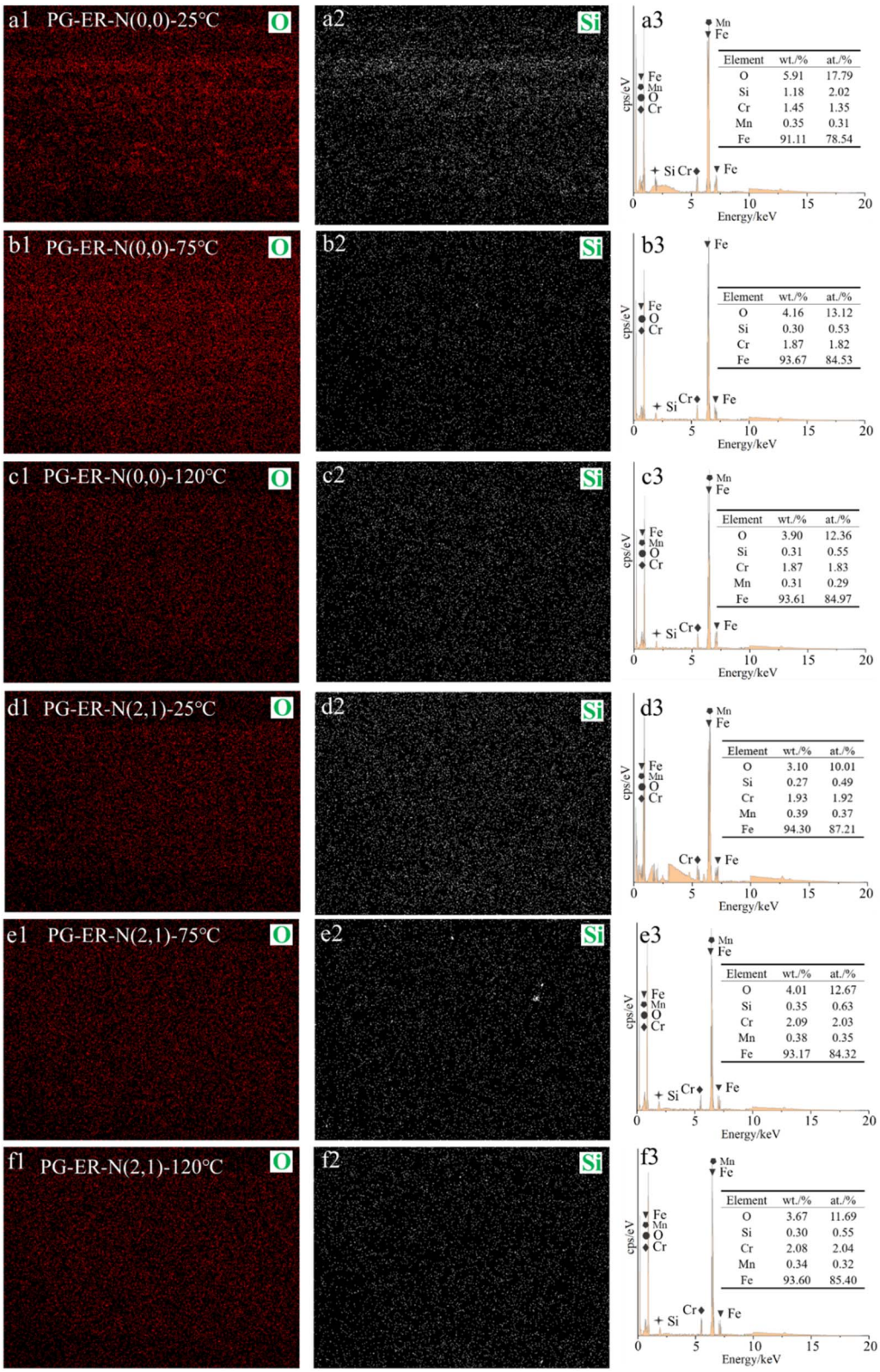

Fig. 5 EDS analyses of the GCr15 steel surfaces lubricated with the PG-ER-N (0, 0) series greases (a1–a3, b1–b3 and c1–c3) and PG-ER-N (2, 1) series greases (d1–d3, e1–e3 and f1–f3) at different temperatures.

N(2, 1) is superior to that of PG-ER-N(0, 0), and both greases exhibit high temperature sensitivity, with friction-reducing performance improving at elevated temperatures.

As shown in Fig. 4(b and c), at 75 °C and 120 °C, the surfaces of PG-ER-N(0, 0)-75 °C and PG-ER-N(0, 0)-120 °C exhibit numerous grooves of varying depth and minor wear debris,

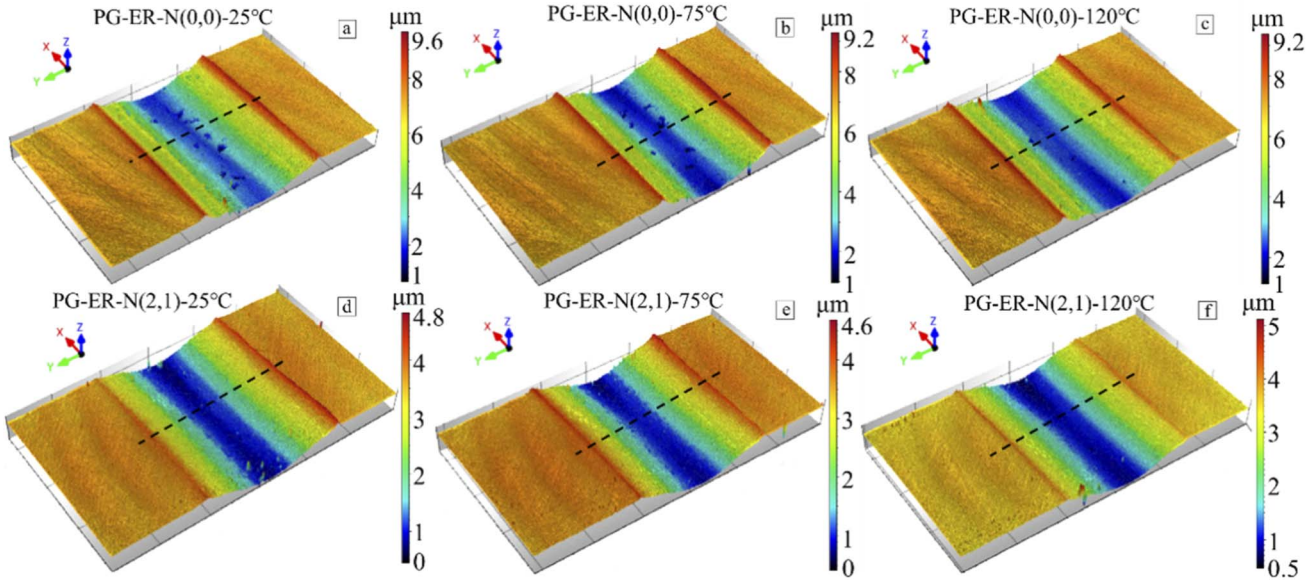

Fig. 6 3D surface morphologies of GCr15 steel samples lubricated with the PG-ER-N (0, 0) series greases (a–c) and PG-ER-N (2, 1) series greases (d–f) at different temperatures.

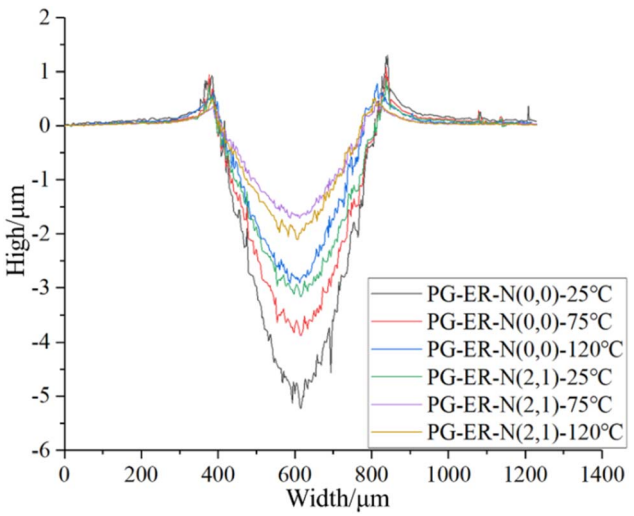

Fig. 7 Profile curves of the wear tracks on GCr15 steel samples lubricated with the PG-ER-N series greases at different temperatures.

indicating abrasive wear. The corresponding EDS maps (Fig. 5b1–b3 and c1–c3) show the presence of O but no increase in Si, suggesting oxidative wear. The improved performance at higher temperatures is attributed to the enhanced flowability of PG-ER-N(0, 0) grease, which facilitates the formation of a lubricating film composed of the lamellar polyurea thickener and base oil on the sample surfaces, reducing wear and oxidation.

For PG-ER-N(2, 1) grease, as shown in Fig. 4(d–f), under 25 °C, 75 °C, and 120 °C conditions, the surfaces exhibit grooves and wear debris of varying severity, indicating abrasive wear. However, the extent of wear is significantly lower than that observed for PG-ER-N(0, 0)-lubricated samples. EDS analyses (Fig. 5d1–d3, e1–e3 and f1–f3) reveal the presence of O without an increase in Si, indicating oxidative reactions. The superior performance of PG-ER-N(2, 1) grease is attributed to the enhanced flowability at elevated temperatures, which promotes the formation of a thicker lubricating film. The addition of 2 wt% ER and 1 wt% *N*-PAN further increases the film thicknesses (Fig. S1) and reduces oxidation (Table S1), leading to a more pronounced friction-reducing effect compared with PG-ER-N(0, 0) grease.

To further investigate the lubricating performance of the PG-ER-N series greases at different temperatures, the 3D surface morphologies and corresponding profilometry curves of the samples were analyzed, as shown in Fig. 6. The surface roughness parameters of the samples were also evaluated, as presented in Fig. 7.

As shown in Fig. 6 and 7, the wear tracks on the surfaces of GCr15 steel lubricated with the PG-ER-N series greases are deep and narrow at different temperatures. The amplitude of the profilometry curves decreases with increasing temperature, and the PG-ER-N(2, 1) has a smoother profile with the minimum wear rate (Table S3). These results indicate that polyurea greases are suitable for high-temperature lubrication, effectively reducing surface wear, and that the addition of 2 wt% ER and 1 wt% *N*-PAN further enhances the lubricating performance.

To further investigate the lubricating performance of the PG-ER-N series greases from different perspectives, the cross-sectional wear profiles of the sample wear tracks were analyzed, as shown in Fig. 8.

As shown in Fig. 8, at the same temperature, the wear on the surfaces of samples lubricated with PG-ER-N(2, 1) is less severe than that on samples lubricated with PG-ER-N(0, 0). From Fig. 8(a), the cross-section of the wear track on the PG-ER-N(0, 0)-25 °C sample exhibits delamination and severe spalling, resulting from both abrasive and adhesive wear. In Fig. 8(b–f), the cross-sections of the wear tracks show numerous regular transverse cracks, corresponding to the grooves observed on the sample surfaces (Fig. 4).

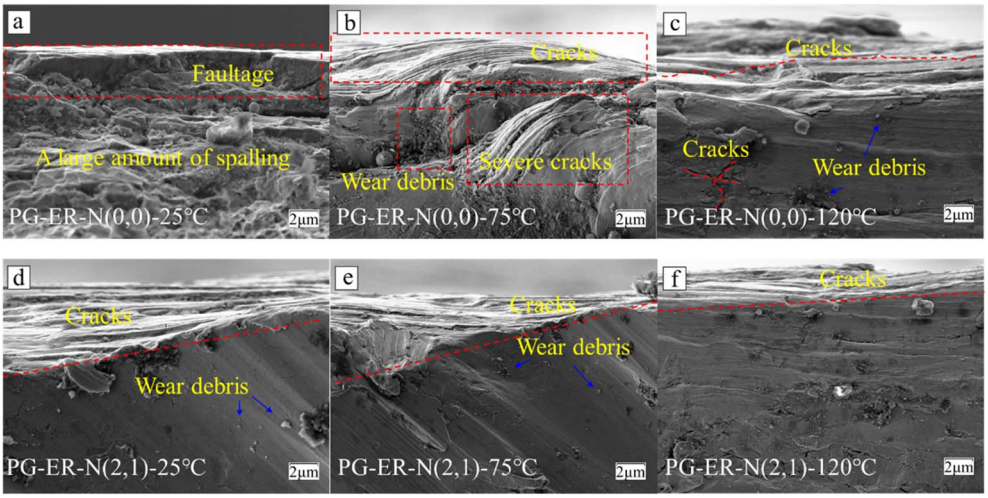

Fig. 8 SEM images of the cross-sections of wear tracks on GCr15 steel samples lubricated with the PG-ER-N series greases (a–c) and PG-ER-N (2, 1) series greases (d–f) at different temperatures.

3.3 Lubrication mechanism analysis

The proposed lubrication mechanism of the PG-ER-N series greases at different temperatures is illustrated in Fig. 9. The schematic of the reciprocating friction test is shown in Fig. 9e, and the tribological characteristics and surface profiles of GCr15 steel lubricated by the PG-ER-N greases are presented in Fig. 9d. The lubricating film formed between the GCr15 steel and Si_3N_4 ball consists of base oil, polyurea thickener, and additives (ER or *N*-PAN).

In polyurea greases, intermolecular aggregation mainly occurs through hydrogen bonding, π–π stacking, and van der Waals interactions, forming fibrous and lamellar structures of varying lengths (Fig. 2b and c). As the temperature rises to 75 °C

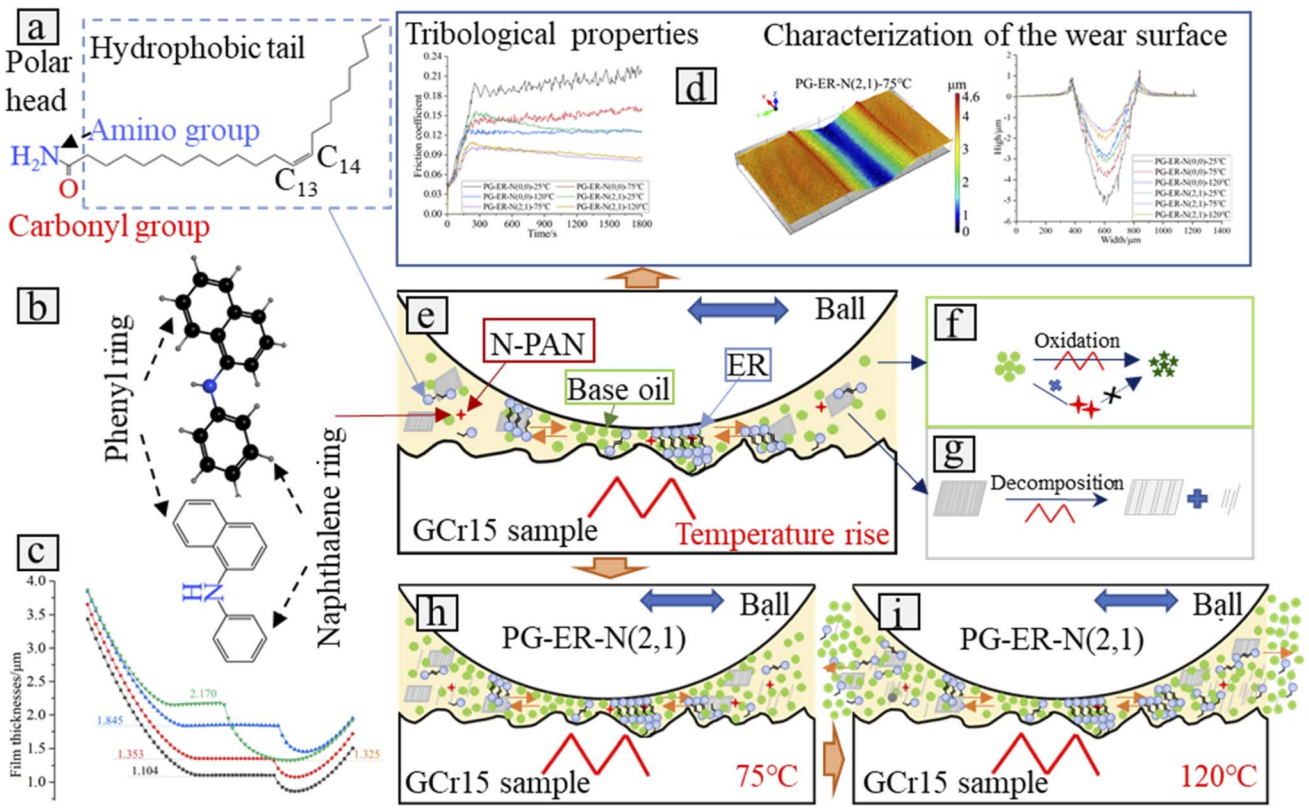

Fig. 9 Lubrication mechanism models of the PG-ER-N series greases on GCr15 steel at different temperatures ((a) ER molecular formula; (b) PANA molecular formula; (c) lubricating film thickness; (d) tribological performance and wear characterization; (e) lubrication model; (f) PANA antioxidant process; (g) polyurea thickener decomposition; (h) lubrication model of PG-ER-N(2, 1) at 75 °C; (i) lubrication model of PG-ER-N(2, 1) at 120 °C).

(Fig. 9h), when the applied shear force exceeds the yield stress, hydrogen bonds, π–π stacking, and van der Waals forces within the polyurea thickener are partially broken. Consequently, base oil, ER, and *N*-PAN are released and spread over the frictional interface. When the shear stress is removed, the thickener undergoes self-reorganization: hydrogen bonding plays a dominant role, π–π stacking provides structural cooperation, and van der Waals forces assist weak molecular interactions. Together, these interactions enable the thickener to self-heal, rebuild the supporting network, encapsulate the base oil, and prevent lubricant loss.

Meanwhile, 2 wt% ER molecules form an ordered bilayer structure through hydrogen bonding between amide groups (–NH_2 and C═O) and π–π stacking between olefinic chains, enhancing the compactness and adhesion of the lubricating film (Fig. 9a). Chemically, the hydrophobic alkyl tail of ER reduces interfacial energy and improves the thermal and shear stability of the lubricating film. Physically, the "head-to-head, tail-to-tail" bilayer arrangement facilitates a transition from sliding friction to rolling friction, significantly reducing friction and wear.[45,46]

In addition, *N*-PAN (*N*-phenyl-α-naphthylamine) contains both benzene and naphthalene rings, forming a conjugated π-electron system with excellent electronic delocalization properties. The hydrogen atoms in *N*-PAN exhibit higher reactivity toward oxygen than hydrocarbon hydrogens, effectively interrupting the oxidation chain reaction of PAO base oil and minimizing free radical formation at elevated temperatures[47] (Fig. 9b and f). As confirmed by Fig. 2 and Table S1, the incorporation of *N*-PAN markedly enhances the oxidation resistance and thermal stability of the lubricating film, thereby extending the grease's service life from a chemical standpoint.

The synergistic effects of ER and *N*-PAN yield a stable and uniform lubricating film (Fig. 9c), preventing direct contact between the friction pairs and effectively reducing friction and wear. However, at 120 °C (Fig. 9i), continuous decomposition of the polyurea thickener (Fig. 9g) occurs. The partial rupture of hydrogen bonds and van der Waals interactions weakens the thickener's self-healing ability, while the increased loss of base oil and ER molecules leads to partial film breakdown. Consequently, the lubrication performance deteriorates, and the friction coefficient rises.

4 Conclusion

This study systematically investigated the tribological performance of polyurea grease and polyurea grease containing ER and N at different temperatures. Based on the results, the following conclusions can be drawn:

(1) Polyurea grease exhibits excellent high-temperature tribological performance, with friction-reducing ability improving as temperature increases. The addition of 2 wt% ER and 1 wt% N further enhances the friction-reducing effect, especially under high-temperature conditions, with the best performance observed at 75 °C.

(2) The polyurea thickener consists of rod-like fibers of varying lengths, forming extensive lamellar structures. Intermolecular interactions, including hydrogen bonding, π–π stacking, and van der Waals forces, assemble the fibers into a supportive "skeleton," which adsorbs the base oil and additives. The 2 wt% ER arranges into a bilayer structure, filling base oil voids and converting sliding friction into rolling friction, while 1 wt% N provides antioxidant protection to reduce oxidation. The combined effects result in optimal friction reduction.

(3) The findings provide support for the application of polyurea grease containing ER and N in bearing materials under high-temperature conditions, demonstrating superior tribological performance. However, the friction-reducing effect of ER and N at high temperatures has limitations, suggesting further exploration to expand the effective temperature range.

Author contributions

Qingchun Liu: writing – original drat review and editing, methodology, and investigation. Wuxin Yu: writing – review & editing, data curation, formal analysis, supervision and resources. Yimin Mo: writing – review & editing, resources. Jun Wang, Changye Liu, Ye Hong, and Qiang Zhang: software and investigation. Fengjie Chen: writing – review & editing, resources.

Conflicts of interest

The authors declare that they have no known competing financial interests or personal relationships that could have appeared to influence the work reported in this paper.

Data availability

The datasets generated and/or analyzed during the current study are available from the corresponding author upon reasonable request. Detailed data supporting the findings of this study, including raw and processed data, can be obtained from the corresponding author, Wuxin Yu, upon reasonable request.

Supplementary information (SI): experimental results, physicochemical measurements, and tribological test outcomes. See DOI: https://doi.org/10.1039/d5ra06889d.

Acknowledgements

We acknowledge the financial support provided by the State Key Laboratory of Precision Blasting, Jianghan University (No. PBSKL2022301), the Research Fund of Jianghan University (No. 2024JCYJ09).

References

1 M. Zheng, G. Ren, S. Wang, Y. Li and M. Xing, Investigating the effect of overbased sulfonates on calcium sulfonate complex grease: enhancements in physicochemical, rheological, and tribological properties, *RSC Adv.*, 2024, **14**(45), 32992–33006, DOI: 10.1039/D4RA04307C.

2 K. Li, Y. Zhang, W. Tan, J. Wang, Z. Xu, Z. Li, *et al.*, Investigation of friction and vibration performance of lithium complex grease containing candle soot on aviation electrical machine, *Wear*, 2024, **550–551**, 205401, DOI: 10.1016/j.wear.2024.205401.

3 D. K. Prasad, S. Tiwari, M. Amarnath, H. Chelladurai, B. S. A. Vardhaman, B. Suresh, *et al.*, Influence of MWCNTs, ZnO, and boric acid nanomaterial blend on the tribological and thermal properties of lithium grease, *Tribol. Int.*, 2024, **192**, 109197, DOI: 10.1016/j.triboint.2023.109197.

4 H. Wu, J. Wang, Z. Guo, H. Du, W. Hu, J. Xu, *et al.*, Self-reformed grease thickener network under shear for improving the lubricating performance at elevated temperature, *Tribol. Int.*, 2025, **204**, 110526, DOI: 10.1016/j.triboint.2025.110526.

5 H. L. Li, Q. F. Zeng, M. J. Fan, Z. M. Pang, J. H. Wang and Y. Liang, Recent progress in high-temperature greases: Constitutive relationships, mechanisms, and applications, *Friction*, 2025, **13**(5), 9440951, DOI: 10.26599/FRICT.2025.9440951.

6 X. H. Wu, Q. Zhao, M. Zhang, W. M. Li, G. Q. Zhao and X. B. Wang, Tribological properties of castor oil tris(diphenyl phosphate) as a high-performance antiwear additive in lubricating greases for steel/steel contacts at elevated temperature, *RSC Adv.*, 2014, **4**(97), 54760–54768, DOI: 10.1039/c4ra09466b.

7 R. Yu, H. C. Liu, Q. M. Sun, W. J. Lou, S. M. Zhang, X. B. Wang, *et al.*, Experimental study on ZDDP tribofilm formation in grease lubricated rolling/sliding contacts, *Tribol. Int.*, 2025, **206**, 110594, DOI: 10.1016/j.triboint.2025.110594.

8 K. P. Zhang, H. T. Tang, X. L. Shi, Y. W. Xue and Q. P. Huang, Effect of Ti3C2 MXenes additive on the tribological properties of lithium grease at different temperatures, *Wear*, 2023, **526**, 204953, DOI: 10.1016/j.wear.2023.204953.

9 X. Xu, F. H. Su, H. Yu, R. Z. Liu and Z. B. Xu, Black phosphorus nanosheet dotted with Fe3O4-PDA nanoparticles: A novel lubricant additive for tribological applications, *Tribol. Int.*, 2025, **207**, 110607, DOI: 10.1016/j.triboint.2025.110607.

10 Y. S. Wang, P. Zhang, X. D. Gao and Y. J. Cheng, Rheological and tribological properties of polyurea greases containing additives of MoDDP and PB, *Tribol. Int.*, 2023, **180**, 108291, DOI: 10.1016/j.triboint.2023.108291.

11 H. Fu, G. P. Yan, M. Li, H. Wang, Y. P. Chen, C. Yan, *et al.*, Graphene as a nanofiller for enhancing the tribological properties and thermal conductivity of base grease, *RSC Adv.*, 2019, **9**(72), 42481–42488, DOI: 10.1039/c9ra09201c.

12 M. Niu and J. J. Qu, Tribological properties of nano-graphite as an additive in mixed oil-based titanium complex grease, *RSC Adv.*, 2018, **8**(73), 42133–42144, DOI: 10.1039/c8ra08109c.

13 J. Zhao, G. Y. Chen, Y. Y. He, S. X. Li, Z. Q. Duan, Y. R. Li, *et al.*, A novel route to the synthesis of an Fe3O4/h-BN 2D nanocomposite as a lubricant additive, *RSC Adv.*, 2019, **9**(12), 6583–6588, DOI: 10.1039/c8ra10312g.

14 E. Goti, L. Corsaro and F. M. Curà, Tribo-thermo-electrical investigation on lubricating grease enriched with graphene nano-platelets as an additive, *Wear*, 2024, **542**, 205264, DOI: 10.1016/j.wear.2024.205264.

15 J. J. Jia, X. Lei, K. Han, P. Yue, S. G. Fan, C. L. Zhang, *et al.*, Synergistic adsorption and lubrication mechanism of CeO2 nanoparticle and MoDTC in lithium complex grease, *RSC Adv.*, 2024, **197**, 109819, DOI: 10.1016/j.triboint.2024.109819.

16 H. Guo, F. H. Chen, R. Liu and P. Iglesias, Lubricating Ability of Magnesium Silicate Hydroxide-Based Nanopowder as Lubricant Additive in Steel-Steel and Ceramic-Steel Contacts, *Tribol. Trans.*, 2020, **63**(4), 585–596, DOI: 10.1080/10402004.2019.1710312.

17 C. Wu, K. Yang, Y. Chen, J. Ni, L. D. Yao and X. L. Li, Investigation of friction and vibration performance of lithium complex grease containing nano-particles on rolling bearing, *Tribol. Int.*, 2021, **155**, 106761, DOI: 10.1016/j.triboint.2020.106761.

18 C. Wu, R. F. Xiong, J. Ni, L. D. Yao, L. Chen and X. L. Li, Effects of CuO nanoparticles on friction and vibration behaviors of grease on rolling bearing, *Tribol. Int.*, 2020, **152**, 106552, DOI: 10.1016/j.triboint.2020.106552.

19 P. A. Bonnaud, H. Moritani, T. Kinjo, N. Sato and M. Tohyama, Molecular simulations of amine-based organic additives at a steel surface: Effect of the internal molecular structure on adsorption, *Tribol. Int.*, 2025, **201**, 110258, DOI: 10.1016/j.triboint.2024.110258.

20 R. Gusain and O. P. Khatri, Halogen-free ionic liquids: effect of chelated orthoborate anion structure on their lubrication properties, *RSC Adv.*, 2015, **5**(32), 25287–25294, DOI: 10.1039/c5ra03092g.

21 D. Gubala, R. Harniman, J. C. Eloi, P. Wasik, D. Wermeille, L. L. Sun, *et al.*, Multiscale characterisation of single synthetic fibres: Surface morphology and nanomechanical properties, *J. Colloid Interface Sci.*, 2020, **571**, 398–411, DOI: 10.1016/j.jcis.2020.03.051.

22 N. Dulal, R. Shanks, T. Gengenbach, H. Gill, D. Chalmers, B. Adhikari, *et al.*, Slip-additive migration, surface morphology, and performance on injection moulded high-density polyethylene closures, *J. Colloid Interface Sci.*, 2017, **505**, 537–545, DOI: 10.1016/j.jcis.2017.06.040.

23 R. Narayana, C. Mohana and A. Kumar, Analytical characterization of erucamide degradants by mass spectrometry, *Polym. Degrad. Stab.*, 2022, **200**, 109956, DOI: 10.1016/j.polymdegradstab.2022.109956.

24 N. P. Awasthi, S. K. Upadhayay and R. R. Singh, Kinetic investigation of erucamide sSynthesis using fatty acid and urea, *J. Oleo Sci.*, 2008, **57**(9), 471–475, DOI: 10.5650/jos.57.471.

25 A. Melkar, R. Kumar, V. P. Singh, P. Singh, S. Samanta and S. Banerjee, Effect of antiblock and slip additives on the properties of tubular quenched polypropylene film, *J. Polym. Eng.*, 2022, **42**(2), 100–108, DOI: 10.1515/polyeng-2021-0186.

26 J. D. Silvano, R. Santa, M. Martins, H. G. Riella, C. Soares and M. A. Fiori, Nanocomposite of erucamide-clay applied for the control of friction coefficient in surfaces of LLDPE,

Polym. Test., 2018, **67**, 1–6, DOI: 10.1016/j.polymertesting.2018.02.013.

27 R. Catarino-Centeno, M. A. Waldo-Mendoza, E. García-Hernandez and J. E. Pérez-López, Relationship between the coefficient of friction of additive in the bulk and chain graft surface density through a diffusion process: Erucamide-stearyl erucamide mixtures in polypropylene films, *J. Vinyl Addit. Technol.*, 2021, **27**(2), 459–466, DOI: 10.1002/vnl.21820.

28 C. A. Shuler, A. V. Janorkar and D. E. Hirt, Fate of erucamide in polyolefin films at elevated temperature, *Polym. Eng. Sci.*, 2004, **44**(12), 2247–2253, DOI: 10.1002/pen.20252.

29 Y. Y. Di, S. Zhang, X. Q. Feng and Q. Y. Li, Tuning frictional properties of molecularly thin erucamide films through controlled self-assembling, *Acta Mech. Sin.*, 2021, **37**(7), 1041–1049, DOI: 10.1007/s10409-021-01122-x.

30 Z. Y. He, L. P. Xiong, J. Liu, S. Han, J. Q. Hu, X. Xu, *et al.*, Tribological property study of mercaptobenzothiazole-containing borate derivatives and its synergistic antioxidative effects with N-phenyl-α-naphthylamine, *Lubr. Sci.*, 2019, **31**(6), 239–251, DOI: 10.1002/ls.1458.

31 L. P. Xiong, Z. Y. He, J. Liu, J. Q. Hu, X. Xin, S. Han, *et al.*, Tribological study of N-containing borate derivatives and their synergistic antioxidation effects with T531, *Friction*, 2019, **7**(5), 417–431, DOI: 10.1007/s40544-018-0216-8.

32 J. F. Joly and R. E. Miller, Density functional theory rate calculation of hydrogen abstraction reactions of N-Phenyl-α-naphthylamine antioxidants, *Ind. Eng. Chem. Res.*, 2018, **57**(3), 876–880, DOI: 10.1021/acs.iecr.7b04073.

33 Z. Y. He, L. P. Xiong, J. Liu, S. Han, J. Q. Hu, X. Xu, *et al.*, Tribological property study of mercaptobenzothiazole-containing borate derivatives and its synergistic antioxidative effects with N-phenyl-α-naphthylamine, *Lubr. Sci.*, 2019, **31**(6), 239–251, DOI: 10.1002/ls.1458.

34 S. D. Du, X. J. Wang, R. G. Wang, L. Lu, Y. L. Luo, G. H. You, *et al.*, Machine-learning-assisted molecular design of phenylnaphthylamine-type antioxidants, *Phys. Chem. Chem. Phys.*, 2022, **24**(21), 13399–13410, DOI: 10.1039/d2cp00083k.

35 Q. C. Liu, Y. M. Mo and D. L. Zhang, Effect of friction parameters on tribological properties of erucamide as grease additive on GCr15 steel, *Phys. Chem. Chem. Phys.*, 2024, **146**(3), DOI: 10.1115/1.4063810.

36 Q. C. Liu, Y. M. Mo, J. C. Lv and H. Zhang, Effects of Erucamide and N-phenyl-α-naphthylamine on the friction and torque behaviors of grease on roller bearings, *Lubricants*, 2023, **11**(12), 531, DOI: 10.3390/lubricants11120531.

37 G. L. Ren, C. J. Zhou, X. Q. Fan, M. Dienwiebel, S. Y. Wang and Y. L. Li, Enhancement of polyurea grease performance through graphene oxide-functionalized polyurea thickeners: A novel hydrogen-bond network approach, *Tribol. Int.*, 2025, **201**(110123), DOI: 10.1016/j.triboint.2024.110123.

38 J. Wang, Z. Guo, W. Hu, X. Li, H. Lu and J. Li, Improving the Oil Separation of Composite Lubricating Polyurea Grease via Regulating the Thickener Network Structure, *Macromolecules*, 2024, **57**(11), 5486–5496, DOI: 10.1021/acs.macromol.4c00101.

39 P. Ding, W. Cao, Q. Ding, C. Liu, W. Yu and L. Hu, An investigation into the microstructure and temperature-dependent evolutionary behavior of polyurea thickeners, *J. Mater. Res. Technol.*, 2025, **35**, 7074–7083, DOI: 10.1016/j.jmrt.2025.03.053.

40 G. Ren, C. Zhou, X. Fan, M. Dienwiebel, S. Wang and Y. Li, Enhancement of polyurea grease performance through graphene oxide-functionalized polyurea thickeners: A novel hydrogen-bond network approach, *Tribol. Int.*, 2025, **201**, 110123, DOI: 10.1016/j.triboint.2024.110123.

41 M. Black, T. Van der Wijst, C. F. War and F. M. Bickelhaupt, π-π stacking tackled with density functional theory, *J. Mol. Model.*, 2007, **13**(12), 1245–1257, DOI: 10.1007/s00894-007-0239-y.

42 W.-X. Liu, D. Liu, Y. Xiao, M. Zou, L.-Y. Shi, K.-K. Yang, *et al.*, Healable, Recyclable, and High-Stretchable Polydimethylsiloxane Elastomer Based on Synergistic Effects of Multiple Supramolecular Interactions, *Macromol. Mater. Eng.*, 2022, **307**(10), 2200310, DOI: 10.1002/mame.202200310.

43 Z. Shi, H. R. Zhou, K. R. Guo, H. Nie, X. P. Zhou and Z. G. Xue, Elastomeric electrolytes via thiourethane dynamic chemistry and hierarchical hydrogen-bonding interactions, *Macromolecules*, 2023, **56**(24), 10179–10191, DOI: 10.1021/acs.macromol.3c01695.

44 Y. Liu, J. Li, J. P. Ge and D. L. Zheng, Effect of acid slag treatment on the inclusions in GCr15 bearing steel, *High Temp. Mater. Process.*, 2019, **38**, 760–766, DOI: 10.1515/htmp-2019-0024.

45 D. Gubala, A. Slastanova, L. Islas, P. Wasik, F. Cacho-Nerin, D. F. Sanchez, *et al.*, Effects of erucamide on fiber "Softness": linking single-fiber crystal structure and mechanical properties, *ACS Nano*, 2024, **18**, 5940–5950, DOI: 10.1021/acsnano.4c00114.

46 E. Har-Even, A. Brown and E. I. Meletis, Effect of friction on the microstructure of compacted solid additive blends for polymers, *Wear*, 2015, **328**, 160–166, DOI: 10.1016/j.wear.2025.01.075.

47 J. F. Joly and R. E. Miller, Density Functional Theory Rate Calculation of Hydrogen Abstraction Reactions of N-Phenyl-α-naphthylamine Antioxidants, *Ind. Eng. Chem. Res.*, 2018, **57**(3), 876–880, DOI: 10.1021/acs.iecr.7b04073.